0.1 Definitions

In chapter **??** we numerically solved Euler's rigid body equations in the rotating body frame yielding the evolution of the spin vector $\boldsymbol{\omega}$; this allowed us to observe the dynamics such as precession and alignment without resolving individual rotations. Physical observations of the star are made in the inertial frame and so observers report on quantities calculable from the TOA of pulses. Generating timing models for the phase, they quote results such as timing residuals and the pulsation frequency and spindown. We aim to simulate these physical observables and test the effect of timing noise mechanisms. To do this, we need to transform the solutions of Euler's rigid body equations into observable quantities in the inertial frame. An efficient way to do this is to determine the Euler angles which transform the rotating body frame axis, denoted by (x', y', z'), to the inertial frame axis for which we will use (x, y, z). We will use the Euler angle parameterisation as described by **?**; a schematic of how these angles are constructed is given in figure 0.1.1.
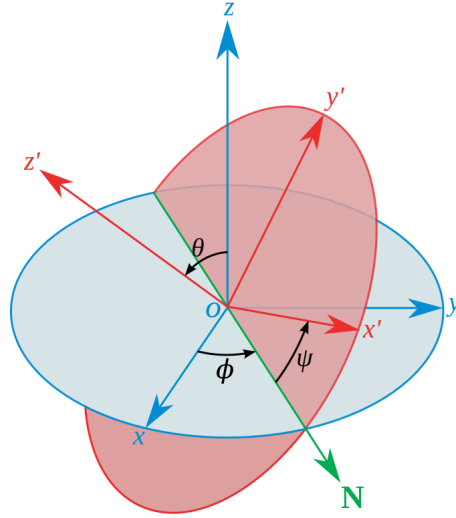

Figure 0.1.1: Schematic of the Euler angle rotation. In the inertial frame the angular momentum is set to lie initially along the z axis. In the rotating body frame for a biaxial body the deformation lies along z' while the spin vector initially lies along in the $x' - z'$ plane.

In the body frame, the diagonal moment of inertia tensor has components I_{xx}, I_{yy} and I_{zz} and the star is spun down by a torque $\boldsymbol{T}$. The Euler rigid body equations are then the left hand side set of equations in (0.1.1). Decomposing the motion of the spin vector into Euler angles and rearranging yields the right hand set of equations in (0.1.1). These describe the evolution of the three Euler angles.

$$\dot{\omega}_x = \frac{1}{I_{xx}} \left[T_x + (I_{yy} - I_{zz}) \omega_y \omega_z \right] \qquad \dot{\theta} = \omega_x \cos\psi - \omega_y \sin\psi$$

$$\dot{\omega}_y = \frac{1}{I_{yy}} \left[T_y + (I_{zz} - I_{xx}) \omega_x \omega_z \right] \qquad \dot{\phi} = \frac{\omega_x \sin\psi + \omega_y \cos\psi}{\sin\theta} \qquad (0.1.1)$$

$$\dot{\omega}_z = \frac{1}{I_{zz}} \left[T_z + (I_{xx} - I_{yy}) \omega_x \omega_y \right] \qquad \dot{\psi} = \omega_z - \dot{\phi}\cos\theta.$$

These equations can be solved numerically using a time stepper, for now we will use the `rkf45` stepper provided by GSL.

0.2 Initial conditions

Solving the rigid body equations in the body frame, we are free to impose the following initial conditions on the spin vector

$$\omega_x = \omega_0 \sin(a_0), \qquad\qquad \omega_y = 0, \qquad\qquad \omega_z = \omega_0 \cos(a_0), \qquad (0.2.1)$$

such that $\boldsymbol{\omega}(t=0)$ lies in the $x' - z'$ plane at an angle a_0 to the z' axis. For a well defined moment of inertia and torque, this is sufficient to solve the rigid body equations.

We now need to consider the initial conditions for the right hand set of equations on (0.1.1). The Euler angles define three rotations which we can combine into a single rotation matrix $R(\theta, \phi, \psi)$. Following the **?** convention this is given by

$$R(\theta, \phi, \psi) = \begin{bmatrix} \cos\psi\cos\phi - \cos\theta\sin\phi\sin\psi & \cos\psi\sin\phi + \cos\theta\cos\psi\sin\psi & \sin\psi\sin\theta \\ -\sin\psi\cos\phi - \cos\theta\sin\phi\cos\psi & -\sin\psi\sin\phi + \cos\theta\cos\phi\cos\psi & \cos\psi\sin\theta \\ \sin\theta\sin\phi & -\sin\theta\cos\phi & \cos\theta \end{bmatrix}$$

$$(0.2.2)$$

Then the angular momentum vectors in the two frames are related by

$$\mathbf{J}_{\mathrm{rot}} = R(\theta, \phi, \psi)\mathbf{J}_{\mathrm{in}}. \qquad (0.2.3)$$

In the body frame, the moment of inertia is constant and since we have already set the initial condition on $\boldsymbol{\omega}$ in equation (0.2.1) the initial angular momentum is

$$\mathbf{J}_{\mathrm{rot}}(t=0) = I\boldsymbol{\omega}_0. \qquad (0.2.4)$$

If we set an initial condition on the angular momentum in the inertial frame, we uniquely define the initial Euler angles. Therefore we choose to set the initial angular momentum in the inertial frame to lie along the inertial z axis such that

$$\mathbf{J}_{\mathrm{in}}(t=0) = |J|\mathbf{z} \qquad (0.2.5)$$

Inserting the magnitude of the angular momentum as $|\boldsymbol{J}| = |I\boldsymbol{\omega}_0| = \omega_0\sqrt{(I_{xx}\sin a_0)^2 + (I_{zz}\cos a_0)^2}$ then from equation (0.2.3) we have

$$\begin{bmatrix} I_{xx}\sin a_0 \\ 0 \\ I_{zz}\cos a_0 \end{bmatrix} = \sqrt{(I_{xx}\sin a_0)^2 + (I_{zz}\cos a_0)^2} \begin{bmatrix} \sin\psi_0\sin\theta_0 \\ \cos\psi_0\sin\theta_0 \\ \cos\theta_0 \end{bmatrix}. \qquad (0.2.6)$$

We have three equations for two unknowns. Our choice to set $\boldsymbol{J}$ along the z axis leaves the initial value of ϕ a free variable; for simplicity we set it by $\phi_0 = 0$. Considering the third component in equation (0.2.6) and rearranging yields

$$\theta_0 = \arccos\left(\frac{I_{zz}\cos a_0}{\sqrt{(I_{xx}\sin a_0)^2 + (I_{zz}\cos a_0)^2}}\right). \qquad (0.2.7)$$

In the limit $\epsilon_I \ll 1$ we have that $\theta_0 \approx a_0$. For ψ_0, we rearrange the first component of equation (0.2.6)

$$\sin\psi_0 = \frac{1}{\sin\theta_0} \frac{I_{xx}\sin a_0}{\sqrt{(I_{xx}\sin a_0)^2 + (I_{zz}\cos a_0)^2}} \qquad (0.2.8)$$

We can simplify the first term by using the identity $\sin(\arccos(x)) = \sqrt{1 - x^2}$ along with equation (0.2.7) to give

$$\sin \theta_0 = \left(\frac{(I_{xx} \sin a_0)^2}{(I_{xx} \sin a_0)^2 + (I_{zz} \cos a_0)^2} \right)^{1/2} \tag{0.2.9}$$

Inserting this into equation (0.2.8) and rearrange

$$\sin \psi_0 = \frac{I_{xx} \sin a_0}{\left(I_{xx}^2 \sin^2 a_0 \right)^{1/2}} \tag{0.2.10}$$

$$= \frac{\sin a_0}{|\sin a_0|} \tag{0.2.11}$$

$$= \text{sign}(a_0), \tag{0.2.12}$$

where by $\text{sign}(x)$ we take the sign of x. Then for the initial condition we have

$$\psi_0 = \text{sign}(a_0) \frac{\pi}{2}. \tag{0.2.13}$$

This result makes sense since inserting it into the second component of equation (0.2.6) balances the right hand side.

0.3 Biaxial body with no torque

The precession of a spinning biaxial body free from torques can be described as the superposition of two rotations. The fast rotation due to the spin of the star and a slower precession about the symmetry axis. Decomposing the motion into the Euler angles **?** demonstrated that: the wobble angle θ remains fixed; the azimuthal angle ϕ monotonically increases at the 'spin frequency' $\dot{\phi}$; the body frame precession refers to the decrease (for oblate bodies) of ψ at the slower precession frequency $\dot{\psi}$. So with the initial conditions the analytic solutions take the form

$$\theta(t) = \theta_0 \approx a_0 \tag{0.3.1}$$

$$\phi(t) = \dot{\phi}t + \phi_0 = \omega_0 t \tag{0.3.2}$$

$$\psi(t) = \dot{\psi}t + \psi_0 = -\epsilon_I \omega_0 t + \frac{\pi}{2} \tag{0.3.3}$$

We begin by testing that our numerical solutions of equations (0.1.1) is consistent with this description.

0.3.1 Solving the equations

In figure 0.3.1 we present the solution of equation (0.1.1) for some typical values. In the left hand figure, the body frame spherical components are given showing the usual torque-free precession. In the right hand plot, we plot the Euler angles. This demonstrates 'almost' perfect agreement with **?** for the Euler angles of a oblate precessing body. That is, ϕ monotonically increases at the spin frequency while ψ decreases at the slower precession frequency. The polar angle θ should remain constant during this simulation. Inspecting its value however, we find it varies fractional level by $\sim 10^{-11}$. This is caused by the finite numerical precision when calculating the subtraction defined in equation (0.1.1) for $\dot{\theta} = 0$. On short time scales these errors remain small and so the

results hold. Over sufficiently long time scale these errors can accumulate and eventually lead to a complete loss of numerical accuracy. We must therefore be vigilant to ensure this does not occur when considering realistic values.
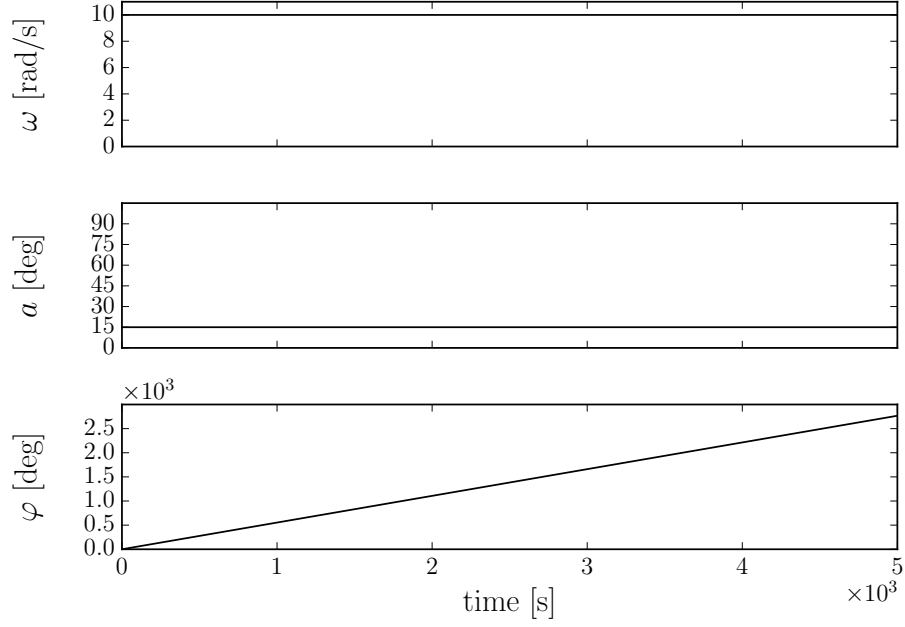
(a) Spherical components in the body frame
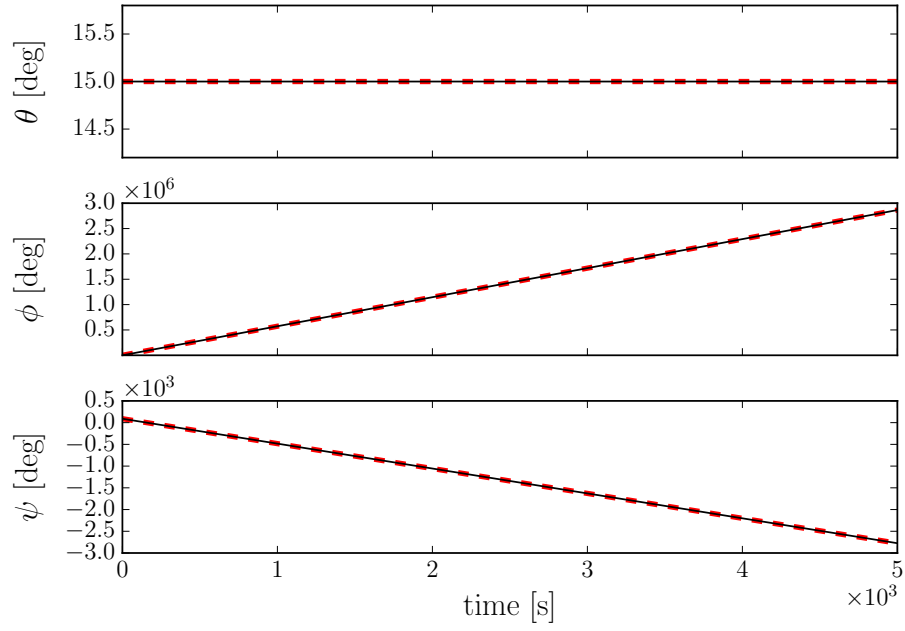
(b) Euler angles

Figure 0.3.1: Solution to the differential equations in (0.1.1) for a canonical biaxial NS with a deformation of $\epsilon_{I3} = 10^{-3}$. The red dashed line is the analytic calculation found by **?** for the evolution of the Euler angles as given in equation (0.3.3).

0.3.2   Physical observables: dynamics of the magnetic dipole

Having the Euler angles allows us to transform from the rotating frame into the inertial frame of an observer. Such an observer will measure the pulses from the electromagnetic radiation that streams out along the open field lines of the dipole $\hat{\boldsymbol{m}}$ as the star rotates. In this model we will assume a thin collimated beam is emitted along the magnetic dipole. In the body frame we set $\hat{\boldsymbol{m}}$ at an angle χ to the z' axis with unit vector $[\sin(\chi), 0, \cos(\chi)]$. Using the Euler angles to transform to the inertial frame, the components are given by

$$\hat{\boldsymbol{m}} = \begin{bmatrix} \cos\phi\cos\psi\sin\chi - \sin\phi\cos\theta\sin\psi\sin\chi + \sin\phi\sin\theta\cos\chi \\ \sin\phi\cos\psi\sin\chi + \cos\phi\cos\theta\sin\psi\sin\chi - \cos\phi\sin\theta\cos\chi \\ \sin\theta\cos\psi\sin\chi + \cos\theta\cos\chi \end{bmatrix}. \tag{0.3.4}$$

Following the work of **?** two angles Φ and Θ are defined to describe the polar and azimuth of $\hat{\boldsymbol{m}}$ in the inertial frame. The azimuthal angle is given by

$$\Phi = \arctan\left(\frac{\hat{\boldsymbol{m}}_y}{\hat{\boldsymbol{m}}_x}\right) = \phi - \frac{\pi}{2} + \arctan\left(\frac{1}{\cos\theta}\left(\frac{\cos\psi\tan\chi}{\tan\theta - \sin\psi\tan\chi}\right)\right), \tag{0.3.5}$$

while the polar angle is

$$\Theta = \arccos(\hat{\boldsymbol{m}}_z) = \arccos(\sin\theta\sin\psi\sin\chi + \cos\theta\cos\chi) \tag{0.3.6}$$

Given a solution of equations (0.1.1) we can use these two equations to describe the evolution of the magnetic dipole orientation in the inertial frame (its magnitude is assumed to be fixed). We will now go on to discuss how this can be related to physical observables.

Instantaneous electromagnetic frequency

An observer sees a pulse from the NS every time the column from the magnetic dipole passes through their location. For the frequency of pulsations, we are interested only in the azimuthal evolution of the magnetic dipole. So we can simplify and say - a pulse will occur every time the magnetic dipole cuts the plane containing the observer and the angular momentum vector $\boldsymbol{J}$. We are neglecting the observers polar position and assuming they do not sit along the spin axis.

Differentiating the phase with respect to time we have

$$\dot{\Phi} = \dot{\phi} + \frac{\sin\chi\left(\dot{\psi}(\cos\theta\sin\chi - \sin\psi\sin\theta\cos\chi) + \dot{\theta}\cos\psi(\cos\theta\sin\chi - \sin\psi\sin\theta\cos\chi)\right)}{(\sin\theta\cos\chi - \cos\theta\sin\psi\sin\chi)^2 + \cos^2\psi\sin^2\chi}. \tag{0.3.7}$$

This is then the *instantaneous electromagnetic frequency*, an observer will measure the time averaged value of $\dot{\Phi}$ as the 'spin frequency' of the star. Recalling that for a biaxial star with no torque θ is constant, **?** found the averaged frequency split into the cases $\theta > \chi$ and $\theta < \chi$.

Understanding the two cases   To get a feeling for the mechanics we can decompose the rotation vector into rotations about the angular momentum and rotation about the deformation axis:

$$\boldsymbol{\omega} = \dot{\phi}\hat{\boldsymbol{n}}_J + \dot{\psi}\hat{\boldsymbol{n}}_d. \tag{0.3.8}$$

Any fixed vector (such as $\hat{\boldsymbol{m}}$) in the body frame can be understood in the inertial frame as undergoing two motions: keeping ϕ fixed and increasing ψ rotates the vector in a cone about the

$\hat{n}_d$ axis; holding instead ψ fixed and increasing ϕ sweeps the vector about a cone centred around the $\hat{n}_J$ axis. Calling these cones the precession and spin cones the resulting motion can be understood as the superposition of the two. **?** found that the types of solutions these cones produced depended on the ordering of θ and χ. In figure 0.3.2 an illustration is given of these cones projected into the reference plane for the three possible orderings of θ and χ.

(a) $\theta > \chi$ (b) $\theta = \chi$ (c) $\theta < \chi$
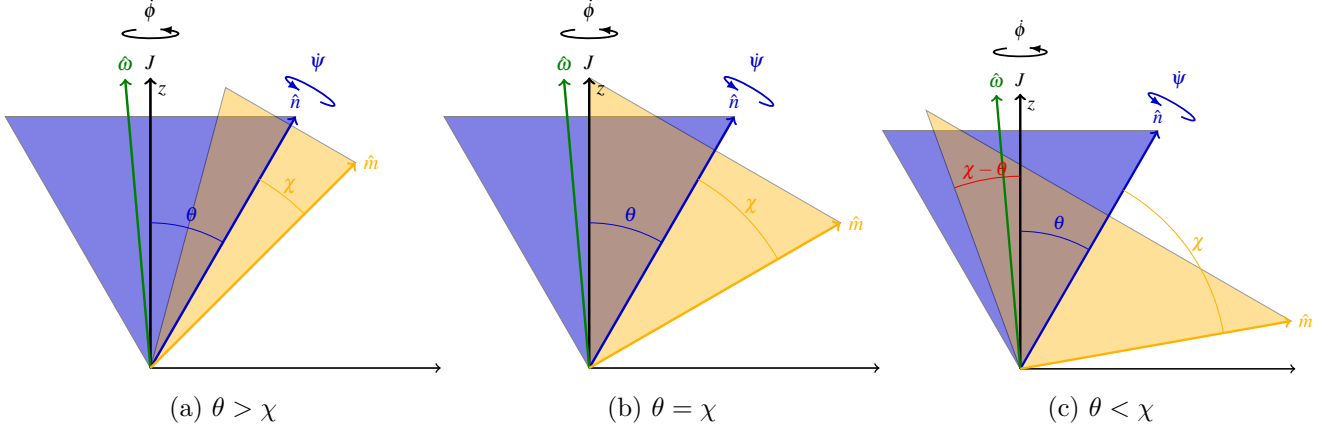
Figure 0.3.2: Diagrams depicting 2D projections of the cones swept out by the different motions under torque free precession onto the reference plane. The yellow cone is swept out by the rotation of $\hat{m}$ about $\hat{n}_d$ at the slow precession frequency; the blue cone is swept out by the rotation of $\hat{n}_d$ about $\boldsymbol{J}$ at the fast spin frequency. The precession cone rotates in the opposing direction to the spin cone for oblate bodies.

The motion of the magnetic dipole about the precession cone evolves on a much longer timescale than its motion about the spin cone; as a result the star will always pulsate once every spin period, but the long precession will modulate the average value on the precession timescale. Because of the large difference in timescales, the motion of $\hat{m}$ can be considered as the slow evolution of a third cone swept out by $\hat{m}$ about $\boldsymbol{J}$ which we will call the dipole cone. The half angle made by this cone is exactly the polar angle Θ calculated in equation (0.3.6). The frequency with which $\hat{m}$ rotates around dipole cone is given by equation (0.3.7). In figures 0.3.3(a) and (b) the polar angle and frequency modulations are plotted for three particular cases, with reference to these plots we now discuss the three cases:

- The $\chi = \theta/2$ case: the precession cone is narrow and does not extend over the angular momentum vector. The polar angle Θ of the dipole cone oscillates periodically between $\theta + \chi$ and $\theta - \chi$ during a precession cycle. The spin frequency $\dot{\Phi}$ has an average value of $\dot{\phi}$ and oscillates about this value, comparing with the Θ variations demonstrates these oscillations are locked in phase with the rotation of $\hat{m}$ in the precession cone. Recalling that the precession cone counter rotates with respect to the spin cone, at $\theta + \chi$ the precession cone motion acts in the opposing direction to the spin cone, this causes a reduction in the spin frequency away from the average; by contrast at $\theta + \chi$ the counter rotation is now in favour of the spin frequency and as a result the spin frequency is increased above the average.

- The $\chi = \theta$ case: here the angular momentum vector sits exactly on the side of the precession cone, this suggest $\hat{m}$ can align exactly with the angular momentum. When this happens the spin frequency tends to zero (due to numerical error, this never actually occurs) manifesting as sharp dips in the spin frequency; at the same time the polar angle tends to zero.

- The $\chi = 4\theta$ case: The precession cone now extends over the angular momentum vector, this means it always acts to reduce the spin frequency; as a result the spin frequency has an average value of $\dot{\phi} + \dot{\psi}$. The polar angle can vary between $\theta + \chi$ and $\chi - \theta$, for χ close to θ the deviations away from the average are large while as χ increases the deviations get smaller as the half angle of the dipole cone increases.
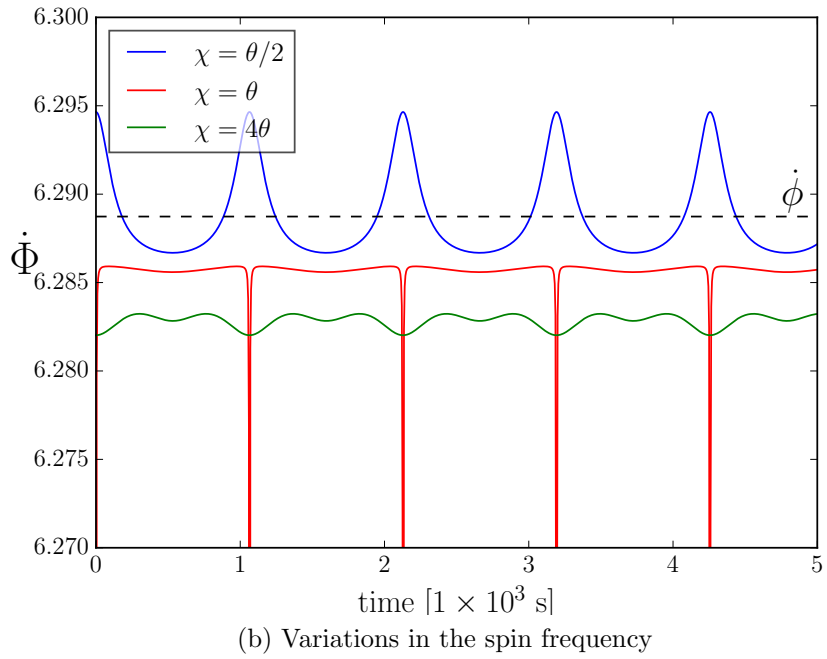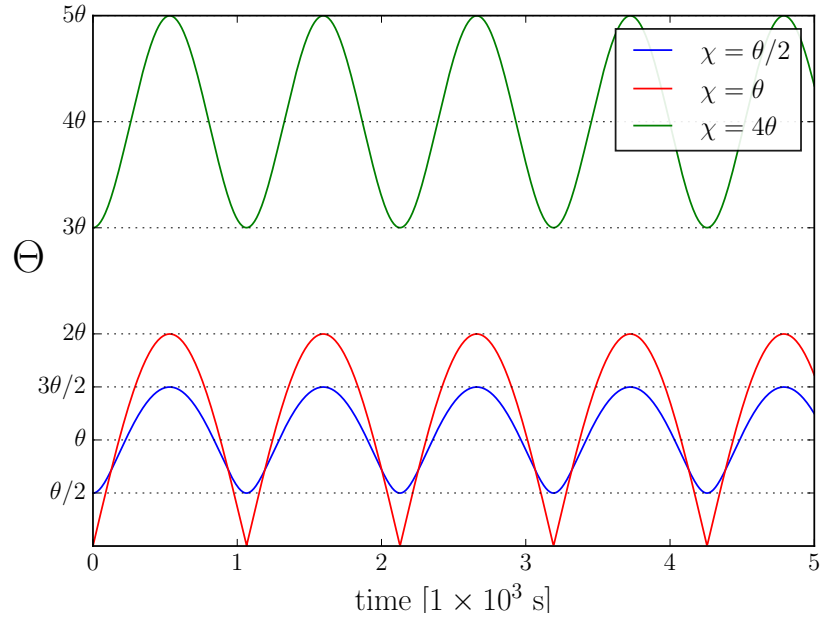
(a) Variations in polar angle

(b) Variations in the spin frequency

Figure 0.3.3

Timing residuals

The principle indicator that a spin down power law does not accurately describe the evolution of pulsars is the structure which exists in the timing residuals. We now aim to introduce the tools required to calculate the timing residuals from our model.

Equation (0.3.5) gives the exact phase evolution of the star, we will label this as Φ_{exact}. We then fit a Taylor expansion truncated at the first order spin to Φ_{exact}. The resulting coefficients, $\dot{\nu}, \nu$ and ϕ_0 are the physical quantities best describing the NS under a power law spindown. Calculating the phase according to this Taylor expansion gives Φ_{fit}, the fitted phase. The residual is then defined as the difference between these two

$$\Delta\Phi = \Phi_{\text{exact}} - \Phi_{\text{fit}} \tag{0.3.9}$$

In figure 0.3.4 we plot the timing residuals as calculated in the torque free model for three values of χ. It is worth noting that the power law spin down assumes that the star is in fact spinning down; without the torque this model can't not spin down. We can however interpret these results as the effect of precession on timing residuals in the limit for which the variation due to precession is much stronger than the spin down. The results show that the precession induces a periodic
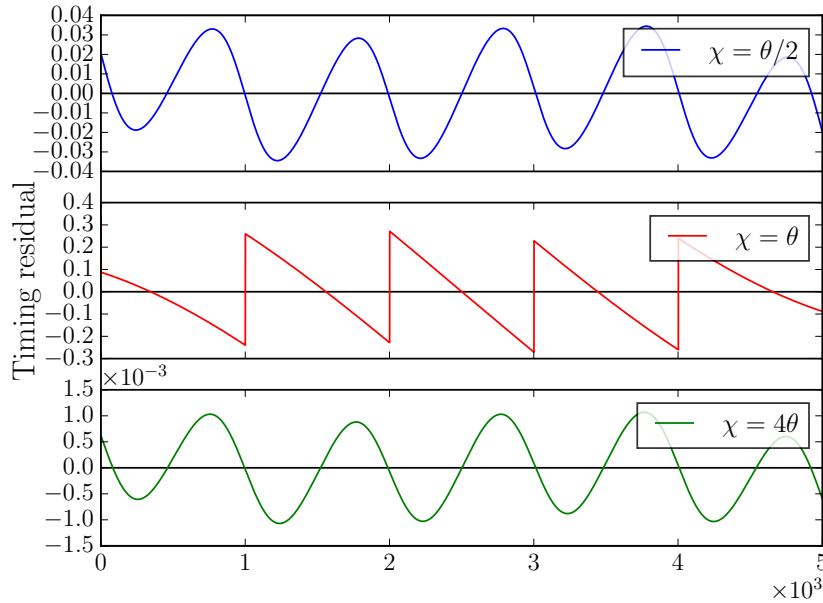

Figure 0.3.4: Plot of the timing residuals for three angles of χ in the torque free model showing different types of behaviour.

variation on the precession timescale, the magnitude is proportional to the angle χ. We also find the results are dependant on the initial angle a_0.

Slowdown Rate $\dot{\nu}$

The second observable which is often considered in characterising periodic patterns in pulsar signals is the slowdown rate. In this simple model the slowdown rate is given by $\ddot{\Phi}$, however calculating an analytic expression is difficult, although possible. As an alternative, we can use the method

10

proposed by Lyne et al. (2010) to measure changes in the spindown of observed pulsars. Second order Taylor expansions are fitted to short sections of data of length T and the resulting coefficient $\dot{\nu}$ is recorded. Repeating this process every $\sim T/4$ through the data set builds picture of how the spindown varies with time. We choose T such that it is a fraction of the precession period over which we expect quantities to be modulated.
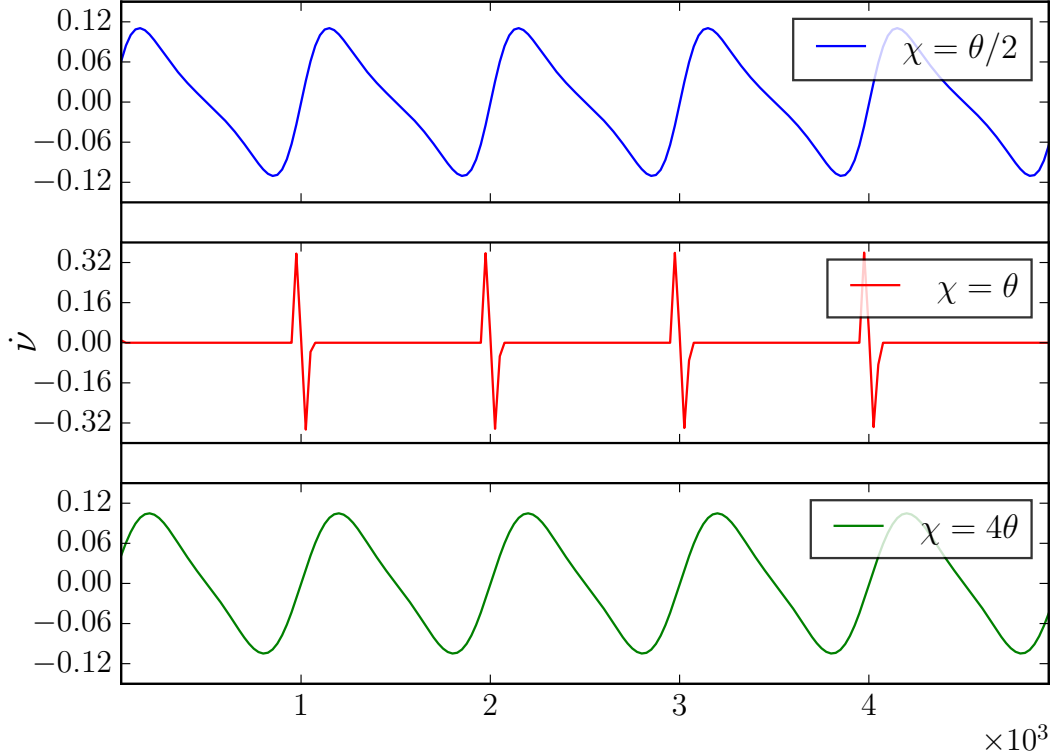

Figure 0.3.5: Slow down rate

The variations seen in figure 0.3.5 are the result of free precession. As there is no torque, the overall spindown is zero. However, due to precession the magnetic dipole performs a slow rotation about the deformation axis. During half the cycle it counter-rotates and in the other half it corotates with the rapid rotation about the angular momentum vector. The result is a symmetric modulation of the spindown about zero. This modulation depends upon the exact geometry. For the $\chi = \theta$ case the cone lies exactly on the spin vector. As such their should be no variation in the spindown. The observed spikes are numerical errors.

Pulse amplitude

Assuming a fixed magnitude of the magnetic dipole, the pulse amplitude will depend on the orientation of the magnetic dipole to the observer and the beam geometry. It will be maximal when pointing directly at the observer and presumably fall off as the angle between the two grows. To model this we take an observers position as Φ_O, Θ_O and then assume the beam geometry follows Gaussian profile with a single conal emmision. This could later be adapted to include a coral emmision.

For such a model of the the beam geometry, the pulse amplitude will vary with the angular separation of the vector from the center of the star to the observer and the magnetic dipole vector. BY considering the intersection of these vectors with the unit sphere, the angular separation can be shown to be

$$\Delta\sigma = \cos^{-1}\left(\sin(\Theta)\sin(\Theta_{\mathrm{obs}}) + \cos(\Theta)\cos(\Theta_{\mathrm{obs}})\cos(\Phi - \Phi_{\mathrm{obs}})\right) \qquad (0.3.10)$$

Then the amplitude of the pulse will be given by

$$A(\Theta, \Phi, \Theta_{\mathrm{obs}}, \Phi_{\mathrm{obs}}, \sigma_B) = A_0 \exp\left(-\frac{\Delta\sigma^2(\Theta, \Phi, \Theta_{\mathrm{obs}}, \Phi_{\mathrm{obs}})}{2\sigma_B^2}\right) \qquad (0.3.11)$$

where A_0 is some constant amplitude, σ_B is a measure of the angular beam width.

In figure 0.3.6 an illustration is given of variations in amplitude from a torque-free pulsar with some arbitary paramaters. This is intended to demonstrate the fast rotation frequency of individual pulses, along with the longer modulation of the precession.
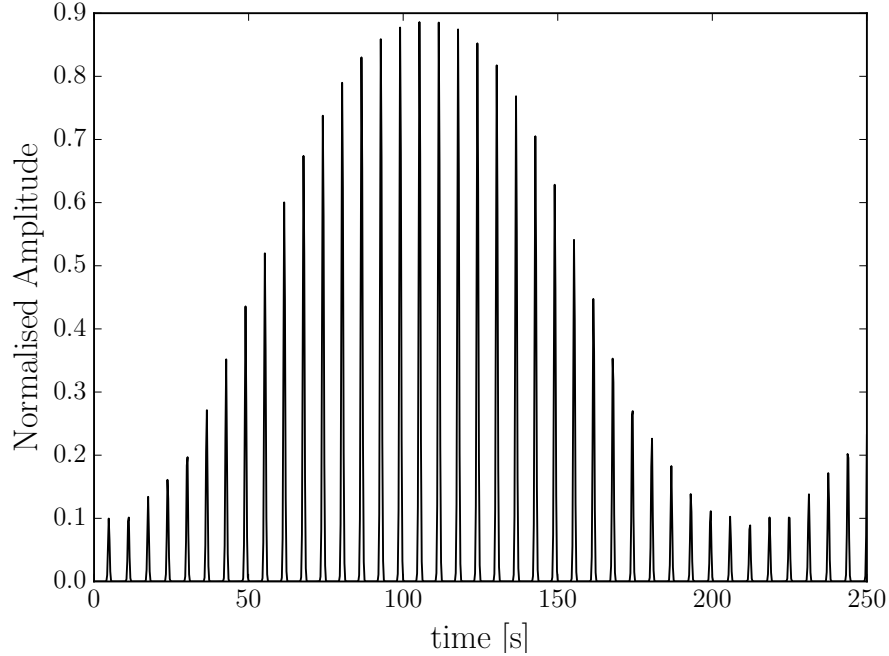

Figure 0.3.6: Amplitude variation using a 2D Gaussian emission.

Pulse width

The amplitude modulations coincide with variations of the pulse width. These have been measured with great accuracy by Lyne et al. (2010) and their correlation with changes in the spindown is key evidence for the two state switching model. We will now extract the pulse width analytically from equation (0.3.11).

To do this we first note that Θ varies on the slow precession timescale, while Φ varies on the rapid spin timescale. We are looking to measure the variations with respect to the slow precession timescale.

The pulse width is measured by the time spent about some fractional amount f of the full pulse amplitude. The condition for when the beam width is greater than this fraction is

$$A(\Phi, \Theta, \Theta_{\text{obs}}, \Phi_{\text{obs}}, \sigma_B) > A_0 \frac{1}{f}. \tag{0.3.12}$$

Substituting equation (0.3.11) and rearranging yeilds

$$\cos(\Phi - \Phi_{\text{obs}}) < \frac{\cos\left(\sqrt{2\sigma_B^2 \ln(f)}\right) - \sin(\Theta)\sin(\Theta)}{\cos(\Theta)\cos(\Theta_{\text{obs}})} \tag{0.3.13}$$

Since we expect Θ to slowly vary, we can over short enough time periods think of it as a constant. Then the whole right hand side of the previous equations is a constant. Lets consider a single rotation with the magnetic dipole starting and ending in the antipodal point to the observers position. Then $\Phi - \Phi_{\text{obs}}$ increase beween $-\pi$ and π during this rotation. The time during which this inequality is true, measures the beam width.

In figure 0.3.7 an illustration is given of this single period showing the constant value on the right hand side of (0.3.13) and the osciallting cosine function. When the cosine is less than this constant this inequality is satisfied. We can calculate the beam width by first measuring the
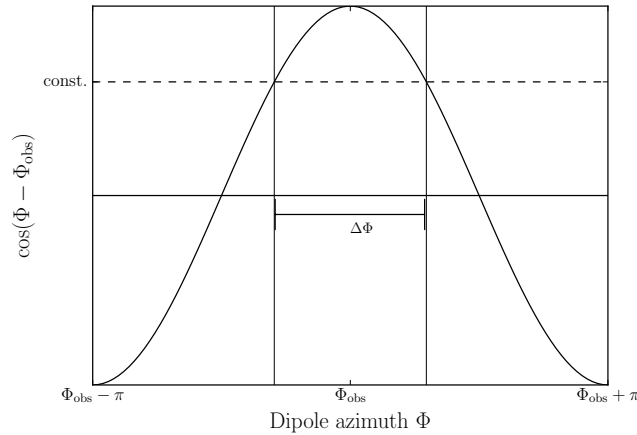

Figure 0.3.7: Illustration of the inequality in equation (0.3.13) the constant value represents the right hand side of this equation. The width $\Delta\Phi$ indicates the angular period during which inequality is satisfied.

angular width $\Delta\Phi$ when the eqeality is not satisified:

$$\Delta\Phi = 2\cos^{-1}\left(\frac{\cos\left(\sqrt{2\sigma_B^2 \ln(f)}\right) - \sin(\Theta)\sin(\Theta)}{\cos(\Theta)\cos(\Theta_{\text{obs}})}\right) \tag{0.3.14}$$

Then the angular fraction at which the inequality *is* satisfied is given by $2\pi - \Delta\Phi$. We can now convert this into a pulse width

$$W_p = T\frac{2\pi - \Delta\Phi}{2\pi} \tag{0.3.15}$$

$$= \frac{1}{\pi\dot{\Phi}}\left(1 - \cos^{-1}\left(\frac{\cos\left(\sqrt{2\sigma_B^2 \ln(\frac{100}{p})}\right) - \sin(\Theta)\sin(\Theta)}{\cos(\Theta)\cos(\Theta_{\text{obs}})}\right)\right) \tag{0.3.16}$$

13

where T is the spin period which we have then written in terms of the spin frequency and p is the percentage of beam width. We should state our notation of W_p is intended to match that of Lyne et al. (2010). This illustrates that the beam width will vary with both the changes in spin-frequency, and with Θ.

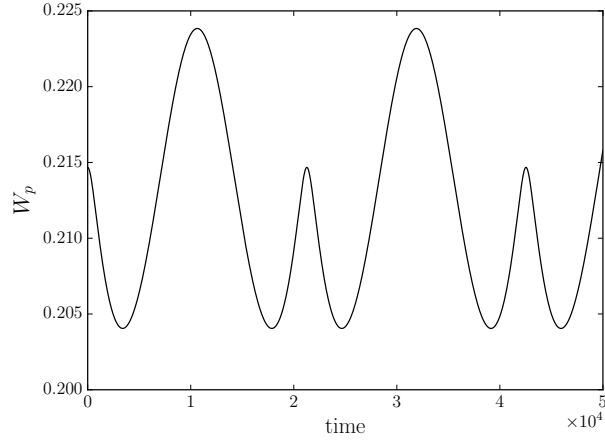In figure 0.3.8 we plot the beam width for some arbitary parameters.

Figure 0.3.8

Bibliography

Lyne, A., Hobbs, G., Kramer, M., Stairs, I., and Stappers, B. (2010). Switched Magnetospheric Regulation of Pulsar Spin-Down. *Science*, 329:408–.